

Research Paper

DOI: <https://doi.org/10.6108/KSPE.2020.24.3.031>

## 초음속 내부유동에서 다수의 충격파 구조에 대한 연구

Jintu K James<sup>a</sup> · 김희동<sup>a,\*</sup>

### Study on Multiple Shock Wave Structures in Supersonic Internal Flow

Jintu K James<sup>a</sup> · Heuy Dong Kim<sup>a,\*</sup>

<sup>a</sup>Department of Mechanical Engineering, Andong National University, Korea

\*Corresponding author. E-mail: kimhd@anu.ac.kr

#### ABSTRACT

The structure and dynamics of multiple shock waves are studied numerically using a finite volume solver for a model with nozzle exit Mach number of 1.75. At first, the shock variation based on images were analyzed using a Matlab program then later to the wall static pressure variation. The amplitude and frequency variation for multiple shock waves are analyzed. The cross-correlation between the shock location suggests that the first and the second shocks are well correlated while the other shocks show a phase lag in the oscillation characteristics. The rms values of pressure fluctuations are maximum at the shock locations while the other parts in the flow exhibit a lower value os standard deviation.

#### 초 록

다수의 충격파에 대한 구조와 거동특성은 노즐 출구 마하수가 1.75인 모델에 대하여 유한체적기법을 사용하여 수치해석적으로 조사하였다. 먼저 이미지를 기반으로 한 충격파 진동특성을 Matlab 프로그램을 사용하여 분석한 후 특정 위치에서 벽면 정압변화를 분석하였다. 또한 다수 충격파들의 진폭 및 주파수도 조사하였다. 충격파 위치들 사이의 상호상관은 첫번째 충격파와 두번째 충격파는 서로 관련이 있는 반면에 다른 충격파들은 진동특성에서 위상 지연을 나타내었다. 벽면 압력변동의 RMS값은 충격파 위치에서 최대이며 유동의 다른 부분에서는 낮은 OS 표준편차값을 나타내었다.

Key Words: Multiple Shock Waves(다수의 충격파), Shock-boundary Layer Interaction(충격파-경계층 간섭), Isolator(격리부), Flow Separation(유동박리), Internal Flow(내부유동)

#### Nomenclature

Received 3 December 2019 / Revised 29 March 2020 / Accepted 31 March 2020

Copyright © The Korean Society of Propulsion Engineers

pISSN 1226-6027 / eISSN 2288-4548

[이 논문은 한국추진공학회 2019년도 추계학술대회(2019. 11. 27-29,

해운대 그랜드호텔) 발표논문을 심사하여 수정·보완한 것임.]

$a$  : Sound velocity

$p$  : Static pressure

$t$  : Time

$T$  : Time period

## 1. Introduction

The supersonic flow in a duct is decelerated to a subsonic flow through a shock train system that is a complex, three-dimensional system of shock and compression waves depending on the boundary conditions. It is essentially a system of coupled shock wave boundary layer interactions. If the duct is sufficiently long, the shock train is followed by a mixing region and the total flow field is termed as the pseudo-shock wave. In this supersonic-subsonic velocity distribution region there exists turbulent mixing that leads to the additional static pressure rise in the flow field. The entire region from the beginning of the shock train to the end of the mixing region is called the pseudo shock [1,2]. The pseudo shock is a critical fluid phenomenon in high-speed air-breathing engines, such as ramjets and dual mode scramjets.

The pseudo shock is generally present in the isolator of the engine which highly coupled with the combustion process and the heat release generates. The pseudo shock must be positioned at a location in the isolator such that the approach flow conditions (i.e., the local flow conditions just upstream of the shock train) can be processed by the shock system to match the downstream boundary condition imposed by the combustor. If the fueling scheme is altered according to the flight requirements, then the pseudo shock responds by moving to a new location in the isolator. Excessive heat release in the combustor may generate a pressure rise that is too large for the pseudo shock to accommodate, and in extreme cases, the shock system propagates upstream until it is disgorged from the inlet in a transient process known as engine unstart. As a consequence,

there is a loss of engine thrust, significantly increased aerodynamic loads, and potentially intense oscillatory flow [3,4]. The main design criteria for an isolator is to generate the amount of pressure rise needed for efficient combustion along with better weight to drag ratio and robustness for a wide range of operating conditions.

The earlier works on pseudo shocks have been studied extensively pointed out that the transition from supersonic to subsonic conditions in ducted flows is normally a complex and gradual flow diffusion process, not a single discontinuity from a normal shock as predicted by inviscid theory. The nature of these shock system depends on Mach number, Reynolds number and, boundary properties. There are several empirical models [5-7] which developed to predict the net changes in the flow properties across the shock system. Recent numerical studies by [8-11] along with experimental background have aided in developing a better understanding of shock train in a duct under different flow conditions.

Fig. 1 shows the schematic of different types of shock trains typically encountered in the pseudo shock system, namely the normal and oblique shock trains adapted from Matsuo et al. [1] and Robin et al [12]. A normal shock train generally has a leading bifurcated normal shock followed by several non-bifurcated shocks. After each normal shock is a re-acceleration region where the core flow speed increases back to supersonic conditions. In an oblique shock train, right-running and left-running oblique shock waves are generated from opposite walls of the duct and cross to form an "X" pattern. Multiple "X" structures form the shock train.

Computational fluid dynamics (CFD) has also been employed to determine the structure

of shock trains. The explicit, time-dependent, second-order accurate MacCormack scheme was used to solve the mass-averaged Navier-Stokes equations [13] by Carroll et al. The computations accurately predicted major features of the shock train in a Mach 1.6 flow, such as centerline Mach number and side-wall pressure, but failed to model the flow separation correctly. Computations by Cox-Stouffer and Hagenmaier solved the three-dimensional Reynolds-averaged conservation equations for perfect gases with a cell-centered finite volume scheme [8]. The results showed that increasing the aspect ratio leads to a longer shock train with the shocks stabilizing further upstream. The trends agree with experimental results, but the numbers were never directly compared. Large-eddy simulations (LES) were carried out by Morgan et al. [10] to model the normal shock train in a constant area duct which compares the experiment of Carroll and Dutton [14]. The LES results showed good agreement in the flow structure when the data was shifted in the stream-wise direction to match the beginning of the shock train in the experiment.

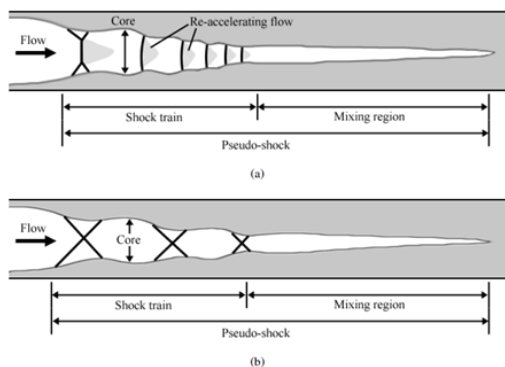


Fig. 1 Schematic of different shock train patterns. (a) Normal shock train, (b) Oblique shock train [12].

Even though there are many works related to shock train, it is not well understood the mechanism and oscillatory characteristics of shock train in detail. This study emphasis on the mechanism and intermittency of shock train oscillations in a constant area duct is analyzed. The goal of the present study is to examine the shock train unsteadiness characteristics and pressure profile. The fluctuations in the static pressure values are analysed to understand the oscillatory characteristics of the shock waves in detail.

## 2. Experimental setup

Experimental studies were conducted in a fully transparent blowdown wind tunnel having a Mach number of 1.75 at the nozzle exit. The nozzle is designed by Method of

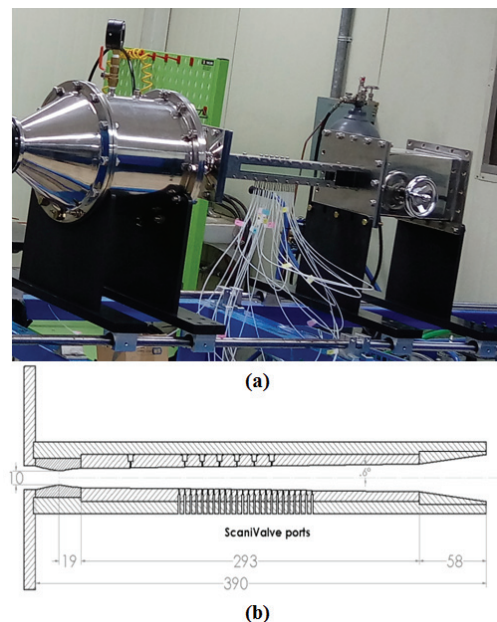


Fig. 2 Details of the experimental facility. (a) Photograph of blow down wind tunnel, (b) Drawing of nozzle-test section assembly.

Characteristics and has a throat height of 10mm, and the whole geometry is having a constant width of 20 mm. The details of the experimental facility are shown in Fig. 2. The photograph of the wind tunnel facility is shown in Fig. 2(a), and the CAD drawing of the nozzle-test section assembly is represented in Fig. 2(b). All the dimensions mentioned are in mm.

The nozzle converges from a height of 40 mm at the inlet to 10 mm at the throat. The quasi parallel test section is a straight line geometry having a length of 292 mm with a diverging angle of 0.6 degrees followed by a divergent section of 58 mm in length and a diverging angle of 4 degrees. The minimal angle in the quasi-parallel section is provided to account for the boundary layer growth, thereby minimizing the pressure gradient in the flow direction. The larger angle at the divergent section stabilizes the shock system due to the large pressure gradient.

The standard Z type Schlieren optical arrangement was used to visualize the movement of shock train in the test section of the wind tunnel. The images were recorded using a Phantom Miro M310 camera. Schlieren optical technique is an extremely useful tool for making an-intrusive measurements of density gradients with high sensitivity and accuracy. The preliminary experiments were done with mirrors having a focal length of 2 m and 200 mm in diameter. The images were taken at a frame rate of 1000 fps and having a size of 440 x 200 pixels with an exposure time of 10  $\mu$ s. The image resolution of the acquisition was measured approximately to be 0.4 mm/pixel.

### 3. Numerical analysis

#### 3.1 Computational domain and boundary conditions

The unsteady CFD simulations were performed for a two-dimensional model as shown in Fig. 3. The 2D simulation can replicate the characteristics of the shock system at the center plane of the test section. The stagnation pressure at the inlet of the isolator is 1.65 bar, and the stagnation temperature is 300 K. At the operating condition, the ratio of stagnation pressure at the inlet to exit is set to be 1.65. The boundary conditions employed in the simulation is also presented in Fig. 3.

The symmetric plane containing the shock train system is considered for the computational analysis, and the flow field is simulated by commercial software FLUENT 19.2. The boundary conditions at inlet and exit are specified as pressure inlet and pressure outlet. Non-slip walls and symmetry boundary conditions have been imposed at the walls and symmetry surface, separately. The steady, two-dimensional, compressible Navier-Stokes equations have been incorporated to simulate the flow field in the duct. The structured grid system is employed in the flow domain with a  $y^+$  value of 1.5. The numerical simulations were carried out in the finite volume solver with density based solver with second order

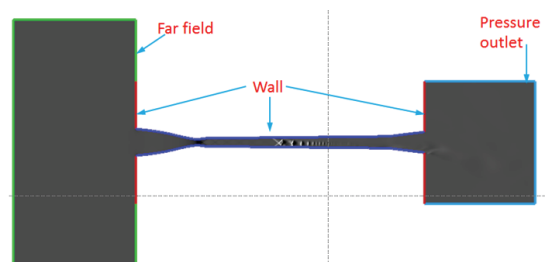


Fig. 3 The geometry details and boundary conditions of the flow field.

upwind spatial discretization. The k- $\omega$  SST turbulence model was used to simulate the physical problem. The working fluid is taken as an ideal gas. The simulations were carried out with a time step size of 1e-06 seconds.

### 3.2 Computational validation

To validate the numerical model, the data obtained from the steady state experimental results are used. The obtained results are plotted in Fig. 4. It can be seen from the figure that the results match very well with a small variation in the shock angle which was formed primarily due to the variation of boundary layer thickness in the flow upstream of the first shock wave. The upper part of the figure represents the numerical Schlieren of the flow field while the bottom one is the corresponding experimental result. The same regions in the flow field were considered for both numerical as well as the experimental results and the flow is from left to right.

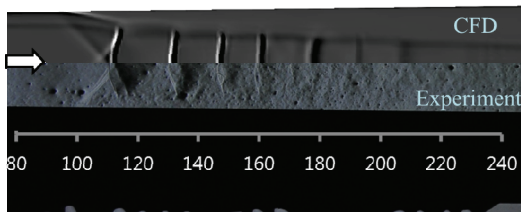


Fig. 4 Comparison of experimental and computational results.

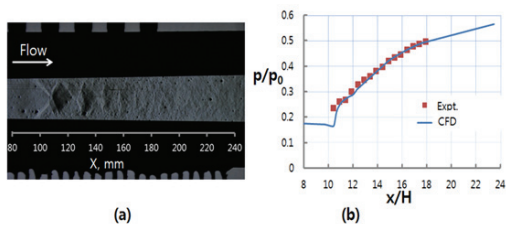


Fig. 5 (a) Schlieren image from experiment and; (b) comparison of wall static pressure between experiment and computation.

The Schlieren images of multiple shock waves and comparison of surface pressure measurements between experiment and computation are shown in Fig. 5. The nozzle throat location is taken as the reference point for measurements. Fig. 5a represents the position of shock train in the rectangular duct while Fig. 5b is the comparison of wall static pressure on the lower wall for experiment and computation.

The pressure on the wall is normalized with inlet stagnation pressure, and shock location is normalized with the throat height of the nozzle. The starting shock location is the same for both computation and experiment. In the real case, the shock will not be stationary, but oscillating even if we maintained a constant pressure ratio across the geometry.

The reliability of unsteady results can be obtained by comparing the obtained numerical results with the experimental results. Fig. 6 represents the comparison of unsteady results.

The upper part indicates the numerical results, while the lower part indicates the

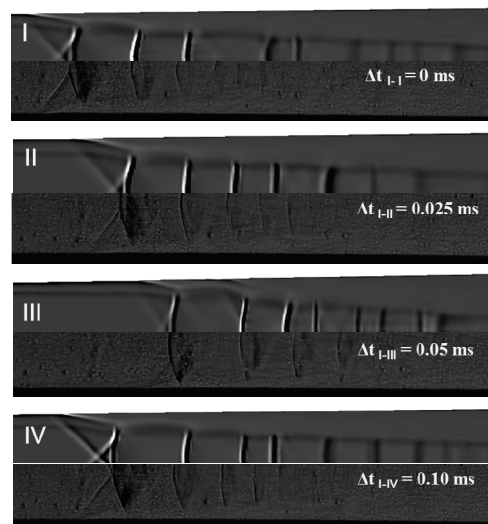


Fig. 6 Comparison of unsteady numerical results with the experimental results.

experimental results. The first image in Fig. 6 is taken as the reference image for the comparison. It is represented at a time of  $\Delta t = 0$  ms. The next image II is taken at a time difference of 0.025 ms for both experimental and numerical schlieren. In other words, both numerical and experimental images are taken at the same interval of time from the reference image. It can be observed that there is a great matching for the shock locations for the upper half and lower half of each image.

#### 4. Results and discussions

##### 4.1 Amplitude of shock train oscillation

Fig. 7 shows the numerical Schlieren of the flow field obtained from the simulation. The multiple shock wave patterns are present in the duct and it is visible. For a constant pressure ratio of 1.65, the shock system is oscillatory and it oscillates about its mean position. Since we are not imposing any changes in the boundary conditions, the oscillations are termed as self-excited oscillations. The characteristics of oscillations are elaborated in the following sessions.

Fig. 8 shows the time variation of the shock locations obtained from the numerical Schlieren images. To obtain the shock locations from images, each image at every time interval is processed using a Matlab image processing code. This code gives the shock location based on the intensity of pixels in the

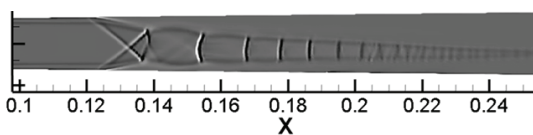


Fig. 7 Numerical Schlieren showing the flow field with multiple shock waves.

images. Thus the shock locations are obtained by taking an appropriate region in the images. The mean location of each shock wave is presented as dotted lines of the same color. It is observed that the distance between mean locations of first and second shock is larger, while the distances between subsequent shocks are reduced.

The fluctuating components or amplitude of each shock system is represented in Fig. 9. The y-axis is obtained by subtracting the mean value of each shock location to its absolute value. The positive value represents that the shock is downstream of its mean position while the negative value corresponds to upstream conditions. It is also noted that the first shock has the maximum amplitude of oscillation, while the other shocks have a lower amplitude of oscillation. It occurs since the second and subsequent shocks are affected

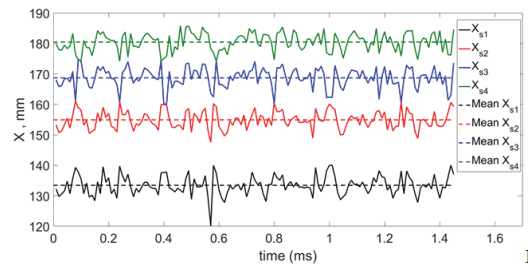


Fig. 8 Variation of the first four shock locations with time. The dotted line in the same color represents the mean value of shock location.

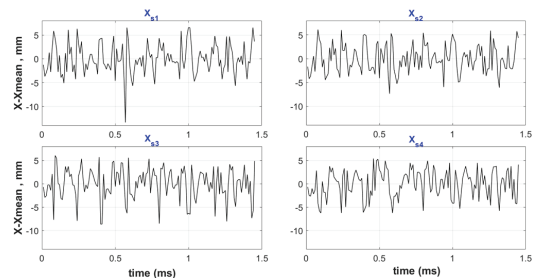


Fig. 9 The variation of the amplitude of the first four shock oscillations to its mean location.

by the pressure fluctuation created by the first shock.

#### 4.2 Relationship between each shocks in the shock train system.

To analyze the response and dependence of each shock with each other, initially cross correlation analysis has conducted. The cross correlation function describes the dependence which one signal has on another, as a function of the delay time between signals. It is determined by taking the average product of  $P_x(t)$  at a time  $t$  and of  $P_y(t)$  at a time  $t+\tau$  over a period  $T$ , as  $T$  approaches infinity.

$$R_{xy}(\tau) = \lim_{T \rightarrow \infty} \frac{1}{T} \int_0^T P_x(t) \cdot P_y(t+\tau) dt$$

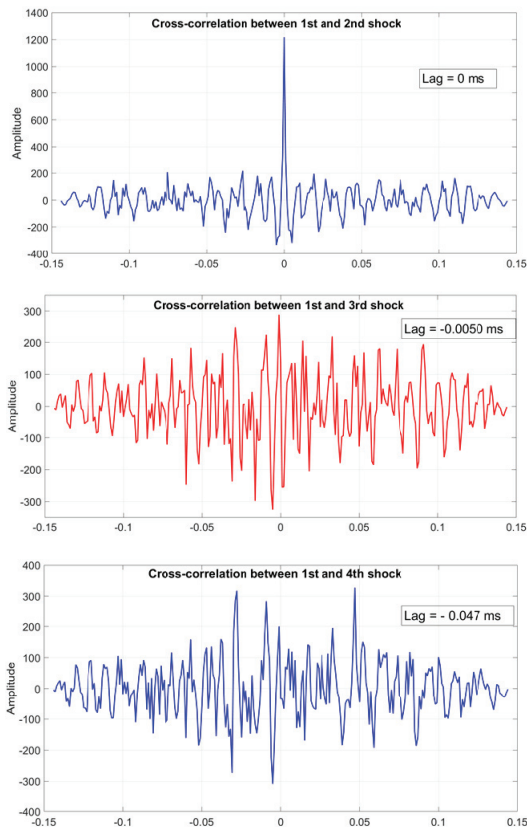


Fig. 10 The cross correlation of shock location with respect to the first shock wave.

One of the most important applications for the cross correlation functions is to determine the time required for a signal source to pass from one point in space to another. The cross correlation between the shock system is presented in Fig. 10. The ordinate represents the value of the correlation between the shock locations. The first and second shocks are well correlated in its amplitude. This means that there is no phase difference in the oscillatory characteristics between them. But the first and third shock correlation suggests that there is a phase difference of  $-0.005$  ms. Or in other words, the third shock lags the first at  $0.005$  ms. The delay between the first shock location and the fourth shock location is  $-0.047$  ms. The delay time corresponds to both the cases are negative. So it may be said that in the low speed region between first shock and the third shock wave, pressure fluctuations propagate in an upstream direction, due to the existence of flow separation region between them. The same trend applies to the first shock and the fourth shock wave. The change in the delay time of the fourth shock arises from the fact that the shock is affected by the pressure fluctuations of upstream shock waves.

#### 4.3 Wall pressure fluctuation in multiple-shock waves

The mean wall static pressure during the simulation is presented in Fig. 11. The lower wall pressure distribution is considered in the present analysis. We can see that there is a pressure increment at  $x=120$  mm which corresponds to the foot of the lambda shock. The pressure rises continuously after the shock train region which is at  $200$  mm, which indicates the mixing region in the flow field. To analyze the pressure fluctuations in detail, six monitor points were considered and are

presented in Fig. 12. The first point P1 at 115 mm is in the undisturbed flow region and the last point P6 at 250 mm is at far downstream location after the mixing region. The other four points at 133 mm, 155 mm, 168 mm, and 180 mm were considered at the mean shock locations.

The variation of wall static pressure in the monitoring points were studied in detail. Fig. 13 shows the time variation of wall static pressure distributions at these monitoring points. The vertical axis is normalized with the upstream stagnation pressure and only fluctuating components are presented with arbitrary units.

The black line corresponding to point P1 does not show any fluctuating component, which means that the shock wave never crosses the point P1. Therefore we can consider this point as the point in the

undisturbed flow. The larger values of normalized pressure fluctuations are observed at point P2, which corresponds to the first shock location. These values are reduced for the following monitoring points.

It is also noted that there is an increment in pressure when the shock wave crosses the monitor point while moving upstream direction. The sudden increment in pressure is observed at this time. Similarly, when shock wave moves downstream of the monitor point, there is a decrement in the wall static pressure at that time.

Fig. 14 shows the FFT plot obtained from the wall static pressure variation for the four shock locations, namely at P1, P2, P3 and, P4. The dominant frequencies of oscillations are in the range of 100 to 350 Hz, which is consistent with the frequency value mentioned in the literature for the self-excited oscillations. It is also observed that wall pressure fluctuations contain strong oscillations of low frequency. Therefore it can be said that wall pressure fluctuations are induced by each shock wave oscillation composed of multiple shock waves.

The streamwise variation of rms values of pressure in the flow field is presented in the Fig. 15. This variation along the lower wall is presented in this figure. The y axis is

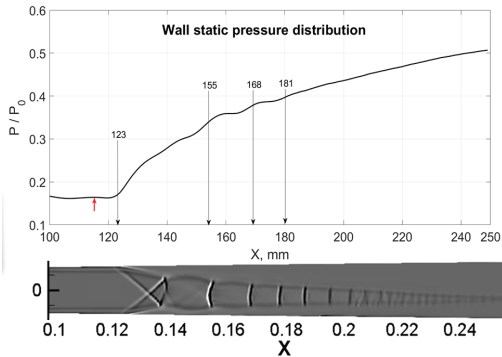


Fig. 11 Wall mean static pressure distribution of the flow field. The lower wall pressure variation is considered.

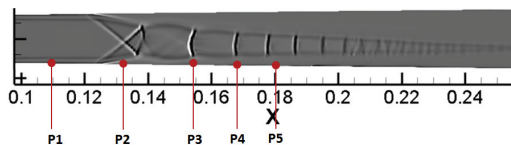


Fig. 12 Pressure fluctuation monitor points on the lower wall of the test section.

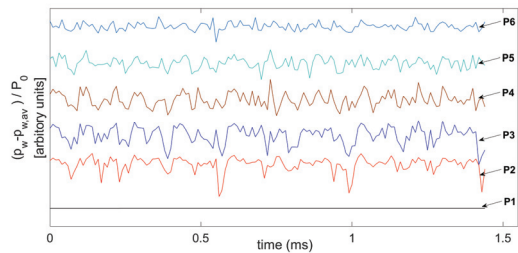


Fig. 13 Time variation of lower wall static pressure at different monitoring points.



normalized with the inlet stagnation pressure. The maximum rms value is observed at the first shock location, where the intermittency due to shock oscillation is very large. The rms values at other shock locations also inhibit a peak in the plot. This shows that the shock oscillations are intermittent. The fluctuation levels downstream of the shock are very likely to be profoundly influenced by the presence of shock-induced separation, and far downstream, the levels are nearly constant.

The first peak is observed at  $x/d = 12.5$  where the first shock wave is present. Ideally, the second peak shock occurs at  $x/D = 15.5$  that corresponds to the mean location of the second shock wave. But we could observe that there is a small peak at  $x/D = 14.2$ . This arises from the presence of shock-induced separation between first and second shock wave. The

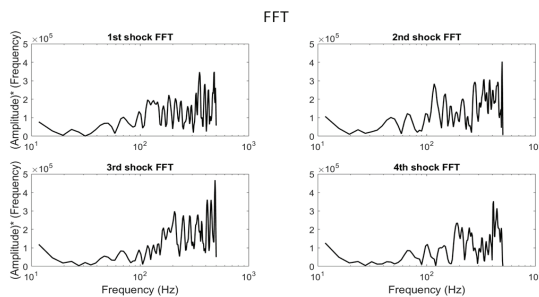


Fig. 14 The FFT plot obtained from pressure variation at first four mean shock locations corresponding to points P1, P2, P3, and P4.

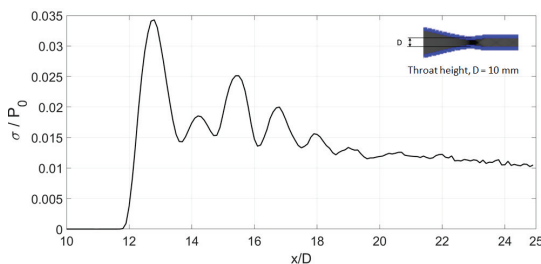


Fig. 15 The streamwise root-mean-square distribution in static pressure on the lower wall.

effect of flow separation is more profound in between the first and second shock waves. The flow separation and hence the induced oscillations are not very evident after the second shock wave. All the pressure fluctuations and the corresponding peaks after the second shock is originated from the oscillation of shock waves alone.

## 5. Conclusions

The characteristic of multiple shock waves in a rectangular channel is investigated computationally and compared with the experimental results. It could be noted that there exists an unsteady oscillation of the shock waves even if the pressure ratio is constant. The cross correlation between the shock location suggests that the first and the second shocks are well correlated while the other shocks show a phase lag in the oscillation characteristics. The amplitude of first shock oscillation is larger compared to other shocks, and it is consistent with shock location as well as the wall pressure measurements. The FFT suggests that the oscillations observed in the simulation are self excited shock oscillations as the fall in the same frequency range mentioned in the literature. The maximum rms value is observed at the first shock location, where the intermittency due to shock oscillation is very large.

## Acknowledgement

This work was supported by the National Research Foundation of Korea (NRF) grant funded by the Korea government (MSIP) (No. NRF-2016R1A2B3016436).

## References

1. Matsuo, K., Miyazato, Y. and Kim, H.D., "Shock Train and Pseudo-shock Phenomena in Internal Gas Flows," *Progress in Aerospace Sciences*, Vol. 35, No. 1, pp. 33-100, 1999.
2. Gnani, F., Zare-Behtash, H. and Kontis, K., "Pseudo-shock Waves and Their Interactions in High-speed Intakes," *Progress in Aerospace Sciences*, Vol. 82, pp. 36-56, 2015.
3. Rodi, P.E., Emami, S. and Trexler, C.A., "Unsteady Pressure Behavior in a Ramjet/Scramjet Inlet," *Journal of Propulsion and Power*, Vol. 12, No. 3, pp. 486-493, 1996.
4. Wagner, J.L., Yuceil, K.B., Valdivia, A., Clemens, N.T. and Dolling, D.S., "Experimental Investigation of Unstart in an Inlet/isolator Model in Mach 5 Flow," *AIAA Journal*, Vol. 47, No. 6, pp. 1528-1542, 2009.
5. Waltrup, P.J. and Billig, F.S., "Structure of Shock Waves in Cylindrical Ducts," *AIAA Journal*, Vol. 11, No. 10, pp. 1404-1408, 1973.
6. Ikui, T., Matsuo, K. and Sasaguchi, K., "Modified Diffusion Model of Pseudo-shock Waves Considering Upstream Boundary Layers," *JSME Bulletin*, Vol. 24, No. 197, pp. 1920-1927, 1981.
7. Smart, M.K., "Flow Modeling of Pseudoshocks in Backpressured Ducts," *AIAA Journal*, Vol. 53, No. 12, pp. 3577-3588, 2015.
8. Cox-Stouffer, S.K. and Hagenmaier, M.A., "The Effect of Aspect Ratio on Isolator Performance," *39th Aerospace Sciences Meeting and Exhibit*, AIAA 2001-0519, 2001.
9. Koo, H. and Raman, V., "Large-eddy Simulation of a Supersonic Inlet-isolator," *AIAA Journal*, Vol. 50, No. 7, pp. 1596-1613, 2012.
10. Morgan, B., Duraisamy, K. and Lele, S.K., "Large-eddy Simulations of a Normal Shock Train in a Constant-area Isolator," *AIAA Journal*, Vol. 52, No. 3, pp. 539-558, 2014.
11. Fiévet, R., Koo, H., Raman, V. and Auslender, A. H., "Numerical Investigation of Shock Train Response to Inflow Boundary-layer Variations," *AIAA Journal*, Vol. 55, No. 9, pp. 2888-2901, 2017.
12. Robin, L.H. and Mirko Gamba, "Shock Train Unsteadiness Characteristics, Oblique-to-normal Transition, and Three-dimensional Leading Shock Structure," *AIAA Journal*, Vol. 56, No. 4, pp. 1569-1587, 2017.
13. Carroll, B., Lopez Fernandez, P. and Dutton, J., "Computations and Experiments for a Multiple Normal Shock/boundary Layer Interaction," *Journal of Propulsion and Power*, Vol. 9, No. 3, pp. 405-411, 1993.
14. Carroll, B. and Dutton, J., "Characteristics of Multiple Shock Wave/turbulent Boundary Layer Interactions in Rectangular Ducts," *Journal of Propulsion and Power*, Vol. 6, No. 2, pp. 186-193, 1990.